

where n is the mean motion, R/a the ratio of lunar radius to semi-major axis, ϵ the obliquity, and l the orbital inclination.

58. C. T. Russell, P. J. Coleman Jr., B. E. Goldstein, *Proc. Lunar Planet. Sci. Conf.* **128**, 831 (1981).
 59. M. J. Wiskerchen and C. P. Sonnett, *ibid.* **1**, 515 (1977).
 60. Y. Nakamura, *J. Geophys. Res.* **88**, 677 (1983).
 61. D. H. Eckhardt, *Moon Planets* **25**, 3 (1981).
 62. The value of x is

$$\frac{(a-c)\left(\frac{18.6 \text{ years}}{27.3 \text{ days}}\right) = \frac{e_c}{0.0040}}$$

63. N. R. Goins, N. M. Toksöz, A. M. Dainty, *Proc. Lunar Planet. Sci. Conf.* **3**, 2424 (1979); N. R. Goins, A. M. Dainty, M. N. Toksöz, *J. Geophys. Res.* **86**, 5061 (1981).
 64. The value of Δk is $k_2(400 \text{ km}) - k_2(300 \text{ km}) = 0.001$.
 65. The core frictional parameter γ is related to the friction coupling parameter K by

$$\gamma = K \left(\frac{18.6 \text{ years}}{27.3 \text{ days}} \right) = \frac{K}{0.0040}$$

where the frictional torque is $Kl_c \omega (\omega - \omega_c)$ and ω and ω_c are the angular velocity vectors of mantle and core, respectively. For turbulent skin friction, K is $(45\pi/32)\kappa \sin \Delta\epsilon$. Here, $\Delta\epsilon$ is the differential obliquity of core and mantle spin vectors and is approximately equal to mantle obliquity (1.54°) for weak frictional and Poincaré pressure coupling. In turn, the local skin friction parameter κ can be derived through simple flat plate theory and is on the

order of 0.001 to within a factor of 2. A 350-km core radius (with core density = 7 g/cm^3) corresponds to $\kappa = 0.0016$.

66. The contribution of solid friction in the moon to the secular dn/dt is

$$\frac{dn}{dt} \approx \frac{9}{2} \frac{k_2}{Q} \frac{M_{\text{Earth}}}{M_{\text{Moon}}} \left(\frac{R}{a} \right)^5 n^2 [7e^2 + \sin^2(l + \epsilon)] = 0.4 \text{ arcsec per century}^2$$

where e is the orbital eccentricity.

67. O. Calame, in (2), pp. 53–63; R. J. Cappallo, R. W. King, C. C. Counselman III, I. I. Shapiro, *Celestial Mech.* **26**, 145 (1982); J. G. Williams, X X Newhall, J. O. Dickey, *Eos* **72** (no. 17), 179 (1991).
 68. S. J. Peale, *J. Geophys. Res.* **81**, 1813 (1976).
 69. D. H. Eckhardt, *Celestial Mech. Dyn. Astron.* **57**, 307 (1993).
 70. P. L. Bender, in *Refraction of Transatmospheric Signals in Geodesy*, J. C. De Munck and T. A. Th. Spoelstra, Eds. (Netherlands Geodetic Commission no. 36, Delft, 1992), pp. 117–125; T. A. Herring, *ibid.*, pp. 157–164. The total atmospheric correction uncertainty given by Bender in Case II of Table 1 is 2 mm at 45° elevation, with one of the two largest contributions being from uncertainties in horizontal gradients. The horizontal gradient effect assumed for Case II is just equal to the total tropospheric horizontal gradient effect for radio waves found by Herring from extensive VLBI measurements. The horizontal gradient contribution should be smaller for laser propagation than for radio waves.
 71. P. L. Bender *et al.*, *Astrophysics from the Moon*, AIP Conference Proceedings 207, M. J. Mumma, H. J.

Smith, G. H. Linebaugh, Eds. (American Institute of Physics, New York, 1990), pp. 647–653.

72. It is impossible to acknowledge all who have been responsible for the achievements described here. The original NASA LURE Team must be listed (in alphabetical order): C. O. Alley, P. L. Bender, D. G. Currie, R. H. Dicke, J. E. Faller, W. M. Kaula, J. D. Mulholland, H. H. Plotkin, E. C. Silverberg, and D. T. Wilkinson. We acknowledge and thank E. C. Silverberg for his pioneering efforts at McDonald Observatory in the early years of the LLR experiment. The success of the early program would not have been possible without the strong support of the late H. J. Smith. We also acknowledge the staffs at CERGA, Haleakala, and McDonald Observatory. We are grateful to K. Nordvedt and T. Damour for comments that improved the manuscript. Normal points were constructed from individual photon returns by R. Ricklefs, P. Shelus, A. Whipple, and J. G. Ries at the University of Texas at Austin for the MLRS and for earlier Haleakala data. D. O'Gara produced later Haleakala normal points. C. Veillet provided normal points for the CERGA data. The work of four of the authors (J.O.D., XXN., C.F.Y., and J.G.W.) presents the results of one phase of research carried out at the Jet Propulsion Laboratory, California Institute of Technology, under contract with the National Aeronautics and Space Administration (NASA). The University of Texas authors (R.L.R., J.G.R., P.J.S., A.L.W., and J.R.W.) acknowledge support from NASA and the U.S. Naval Observatory.

Mobile Point Defects and Atomic Basis for Structural Transformations of a Crystal Surface

Ing-Shouh Hwang,* Silva K. Theiss, J. A. Golovchenko†

Structural transformations on elemental semiconductor surfaces typically occur above several hundred degrees Celsius, and the atomic motions involved are extremely rapid and difficult to observe. However, on the (111) surface of germanium, a few lead atoms catalyze atomic motions so that they can be observed with a tunneling microscope at temperatures below 80°C . Mass transport and structural changes are caused by the creation and propagation of both vacancy-like and interstitial-like point defects within the crystal surface. The availability of dangling bonds on the surface is critical. A detailed atomic model for the observed motions has been developed and is used to explain the structural phase transition $\text{Ge}(111)\text{-c}(2 \times 8) \leftrightarrow 1 \times 1$, which occurs near 300°C .

Interest in diffusion and phase transitions can be said to date back to the earliest days of metallurgy. That interest continues unabated today because our ability to create complex materials with useful properties and the stability of these materials depend

on these phenomena. Both diffusion and structural transformations proceed through mechanisms that operate on the atomic scale, and fundamental understanding has come from indirect methods and reasoning. In single crystals, bulk diffusion is effected primarily by the motion of point defects: vacancies and interstitial atoms (1, 2). A vacancy can move from one substitutional site in a lattice to another and thus lead to mass transport in the opposite direction. An interstitial atom may either diffuse through the lattice until it combines with a vacancy (the interstitial mechanism), or it may replace a substitutional atom, displacing that atom into an adjacent interstitial

site (the interstitialcy or kick-out mechanism). Diffusion that is constrained entirely within a single plane of atoms at a surface may be viewed as the two-dimensional analog of bulk diffusion. It likewise requires mobile point defects. Unlike the bulk, however, the surface is accessible to direct, atomic-scale study. In addition, improved understanding of surface dynamics is of importance in its own right and would benefit disciplines extending from chemistry to electronics.

In recent years, there has been growing interest in the use of the scanning tunneling microscope (STM) for real time and space observations of the fundamental mechanisms of surface mass transport (3–8). One of the main problems in such a study is the slow scanning speed of the current generation of tunneling microscopes, which often cannot follow atomic motions occurring on crystal surfaces. A possible solution is to design STMs that can somehow take images more quickly. Another is to find a way to catalyze the atomic motions such that they occur at lower temperatures, where atomic motions are slower and can be clearly identified by the STM. Such catalysis could be of great practical use as well, for example, in crystal growth.

A small number of impurity Pb atoms on a Ge surface catalyze atomic motions and structural changes without altering the basic mechanisms involved. The present study evolved from our work on Pb atom diffusion, which involves interchanges of individual Pb atoms with Ge adatoms (4). The diffusion tends to occur along the Ge

I.-S. Hwang is with the Division of Applied Sciences, Harvard University, Cambridge, MA 02138, USA. S. K. Theiss is with the Department of Physics, Harvard University, Cambridge, MA 02138, USA. J. A. Golovchenko is with the Department of Physics and Division of Applied Sciences, Harvard University, Cambridge, MA 02138, and Rowland Institute for Science, Cambridge, MA 02142, USA.

*Present address: Institute of Physics, Academia Sinica, Taipei, Taiwan, Republic of China.

†To whom correspondence should be addressed.

adatom row direction, and about half of the interchanges are long jumps (movements of more than one atomic spacing). Additionally, a large number of adjacent Ge adatoms in a row in the $c(2 \times 8)$ surface reconstruction can shift in position concertedly along the row direction like beads on an abacus (5). We have now identified the basic mechanism, which involves mobile point defects, that engenders both surface diffusion and the rich collection of structural transformations the Ge surface harbors.

Here we present STM observations of a lightly Pb-doped Ge(111) surface from 25° to 80°C and of a pure Ge(111) surface from 25° to 220°C. We identify two mobile point defects. One consists of a "partially interstitial" atom in the $c(2 \times 8)$ reconstruction. The other complementary point defect consists of a "partial vacancy" that can alternatively be viewed as a localized high density of surface dangling bonds. The propagation of these two types of mobile point defects is responsible for the structural changes (and mass transport) observed on the Pb-doped Ge(111) surface, and their prolific creation at high temperatures leads to the structural transition $\text{Ge}(111)\text{-}c(2 \times 8) \leftrightarrow 1 \times 1$. Adding a small number of Pb atoms to the Ge(111) surface reduces the activation energy of formation for these two types of mobile point defects and makes their study possible.

Experimental Method

Several features make the lightly Pb-doped Ge(111) surface a favorable one for the STM study of detailed atomic motions. Pb and Ge have negligible mutual bulk solubility at all temperatures (9), and Pb atoms do not evaporate from the surface below 300°C (10). Therefore, Pb atoms remain at the surface after deposition. Furthermore, Pb atoms are easily distinguished from Ge adatoms by the STM and thus can serve as

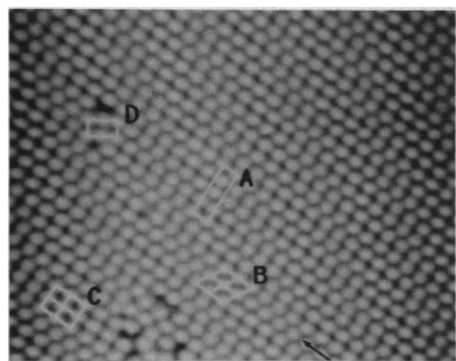


Fig. 1. A 210 Å by 210 Å STM image of a clean Ge(111) surface. Unit cells of (A) $c(2 \times 8)$, (B) 2×2 , and (C) $c(2 \times 4)$ and (D) a defect near a rotated region of $c(2 \times 4)$ are marked. An extra adatom row is indicated with an arrow.

markers, which allow determination of the registry and motion of adatoms.

Our experiments were performed with a homemade STM in an ultrahigh-vacuum chamber with base pressure of 6×10^{-11} torr. Samples of 1- to 5-ohm·cm *n*-type Ge(111) were used. Clean Ge(111)- $c(2 \times 8)$ surfaces were prepared by successive Ne ion sputtering and annealing until very sharp $c(2 \times 8)$ low-energy electron diffraction (LEED) spots were obtained from the entire sample. These surfaces were then either used to study the initial stage of the $c(2 \times 8) \leftrightarrow 1 \times 1$ phase transition on clean Ge(111) or were used as a substrate for Pb deposition. On the latter surfaces, about 0.02 monolayer (one monolayer consists of one Pb atom per first layer Ge atom, a concentration of 7.22×10^{14} cm⁻²) of Pb was deposited from an effusion cell with system pressure below 4×10^{-10} torr. The sample was then transferred to the STM stage. The sample temperature was varied by resistive heating during the experiment. Images were taken between 25° and 80°C for the Pb-doped surfaces and up to ~200°C for the clean surface. Before taking STM images at a new temperature, we waited 30 min to 3 hours to allow the instrument to stabilize thermally. Typically, the STM was operated at a constant current of 20 to 50 pA and with a bias on the sample of about +2 V.

Ge(111)- $c(2 \times 8)$ Reconstruction and Adatom Motions

An STM image of a clean Ge(111) surface at room temperature is shown in Fig. 1. Most of the region has the $c(2 \times 8)$ reconstruction (a unit cell is labeled A). Imperfections in the reconstruction, such as extra adatom rows that result in three rows each of 2×2 (at B) and $c(2 \times 4)$ (at C), can be seen. There is also a small domain of $c(2 \times 4)$ rotated relative to the large domain of $c(2 \times 8)$ (labeled D).

In a perfect Ge(111)- $c(2 \times 8)$ surface reconstruction (Fig. 2), the Ge adatoms occupy the so-called "top, four-coordinated"

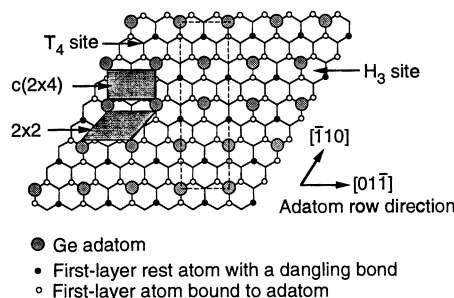


Fig. 2. Simple adatom model of Ge(111)- $c(2 \times 8)$. This reconstruction breaks the three-fold symmetry of the bulk. The adatom row direction is defined as $[01\bar{1}]$. A unit cell is indicated by dashed lines.

sites, or T_4 sites, on the bulk terminated substrate (11–15). Each adatom in a T_4 site forms three bonds to the first layer rest atoms (small open circles in Fig. 2) [it also interacts with the atom directly below it, so this site is considered four-coordinated (Fig. 3)]. The rest atom dangling bonds (RADaBs) (small filled circles in Fig. 2) have the same relative configuration as do the adatoms. A perfect $c(2 \times 8)$ structure has a stacking order along the surface in which rows of 2×2 and $c(2 \times 4)$ subunit cells alternate. The adatom rows are along one of three equivalent $\langle 01\bar{1} \rangle$ substrate directions; thus, there are three possible differently oriented $c(2 \times 8)$ domains, rotated 120° from each other, that break the three-fold symmetry of the substrate. We will refer to the row direction as $[01\bar{1}]$ (Fig. 2).

On the clean Ge(111)- $c(2 \times 8)$ surface, errors in the stacking order can lead to extra adatom rows and result in three (or occasionally four) rows of 2×2 (11, 16). Three adatom rows forming a local $c(2 \times 4)$ arrangement are also seen, but not as often as extra rows of 2×2 . Examination of the model (Fig. 2) reveals that a $c(2 \times 4)$ subunit cell can be converted into a 2×2 subunit cell by shifting all of the atoms on one row to the next T_4 site in the $[01\bar{1}]$ direction. Such adatom row shifts have been observed on the Pb/Ge(111) surface (5). They preserve the $2 \times$ periodicity along the row direction, and we can generally define structures that result from a series of row shifts as "2 × row structures," or "row structures" in brief. The $c(2 \times 8)$, 2×2 , and $c(2 \times 4)$ arrangements are special cases of row structures.

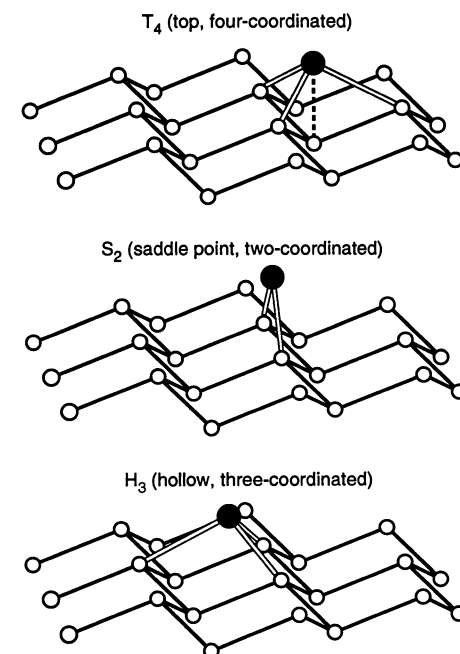


Fig. 3. Model of an adatom movement from a T_4 site to a metastable H_3 site.

An adatom in a "hollow, three-coordinated" site, or H_3 site (Fig. 2), forms three covalent bonds with the substrate as it does on the T_4 site. It has been suggested by Aarts *et al.* (17) that a Ge adatom can move from a T_4 site to a neighboring H_3 site and vice versa by switching only one bond with the rest atoms (Fig. 3). The $T_4 \rightarrow H_3 \rightarrow T_4$ shift is the fundamental mechanism in our model of Ge adatom motions. Recently, first-principles molecular dynamics simulations of the Ge(111)-c(2×8) surface have shown that the energy barrier is 0.8 eV for a Ge adatom to hop from its T_4 site to a neighboring H_3 site and 0.2 eV for it to hop back to the original T_4 site (18). With the Arrhenius equation

$$t = \nu^{-1} \exp(E_D/k_B T) \quad (1)$$

where t is the mean lifetime, E_D is the activation energy, ν is the attempt frequency ($\sim 10^{13} \text{ s}^{-1}$), k_B is the Boltzmann constant, and T is the temperature—we can estimate

the mean lifetime for a Ge adatom to stay at the T_4 site to be several seconds and that on an H_3 site to be 10^{-10} s at room temperature. Because the latter lifetime is 10 to 11 orders of magnitude shorter than the former one, structural changes are very unlikely to occur in the Ge(111)-c(2×8) reconstruction at room temperature. However, they can occur at high temperatures, at which Ge adatoms have a much higher hopping rate to the H_3 site (the hopping rate is the inverse of the lifetime on the T_4 site.)

The motion of a Ge adatom to an H_3 site requires the presence of a RADaB there. If no RADaB is available, the adatom will be unable to switch its bond and the motion is very unlikely to occur (throughout the rest of this article, if Ge motions occur, we assume that the RADaBs are available without always mentioning it specifically). The value of E_D for an adatom to hop from its T_4 site to a neighboring H_3 site varies with the surrounding adatom and RADaB

configuration. Motions involving the simultaneous breaking of two or more Ge–Ge bonds are not considered here because of their high activation energies relative to the highest temperature discussed here (350°C) (19).

Structural Excitations in the Lightly Pb-Doped Ge(111) Surface

When a small quantity of Pb is deposited on Ge(111), most of the Pb atoms replace Ge adatoms in the c(2×8) reconstruction after deposition (4). We call these "substitutional" Pb atoms. A Pb–Ge bond is much weaker than a Ge–Ge bond (5–10). It has been suggested that at room temperature, the substitutional Pb atoms hop rapidly ($>10^3 \text{ s}^{-1}$) between their T_4 sites and the neighboring H_3 sites, with a lifetime on the T_4 sites at least an order of magnitude longer than that on the H_3 sites (5). In contrast, Ge atoms hop to the H_3 site at a

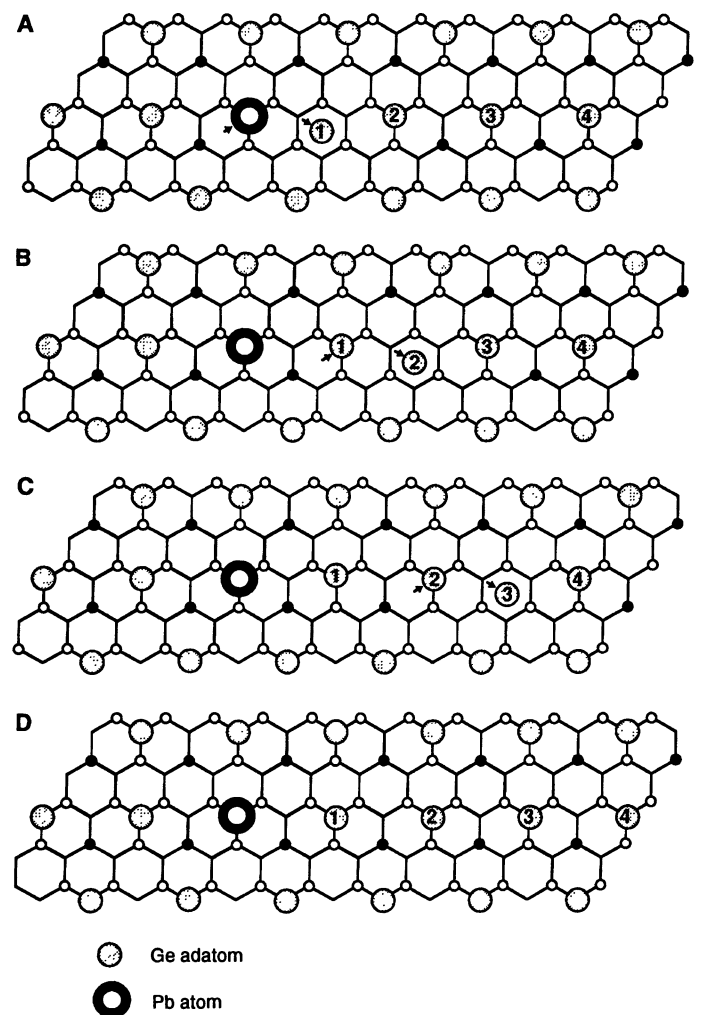
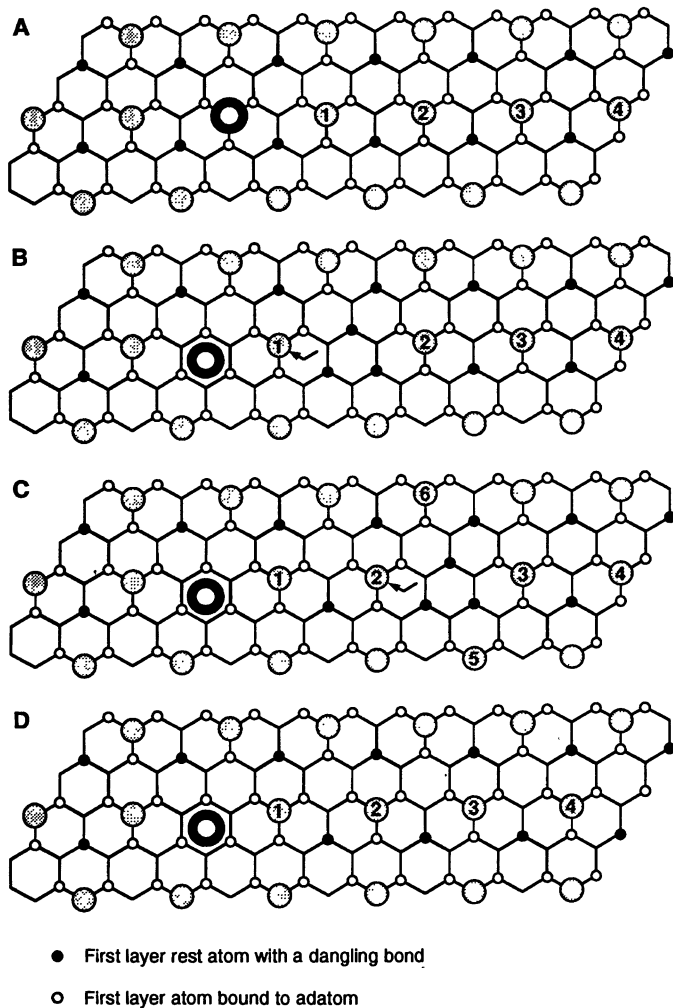


Fig. 4. Model of a vacancy-mediated adatom row shift. (A) Schematic representation of a c(2×8) structure with a substantial Pb atom. (B and C) Intermediate steps in adatom row shift, assuming only that atoms move to nearest-neighbor sites with available RADaBs. (D) Final observed, metastable structure.

Fig. 5. Model of an interstitial site-mediated adatom row shift. (A through C) Intermediate steps in adatom row shift, assuming only that atoms move to nearest-neighbor sites with available RADaBs. (D) Original, observed structure.

rate of about 0.1 s^{-1} , with a lifetime 10 to 11 orders of magnitude longer than that on T_4 . Metastable structures with Pb atoms trapped on the H_3 site were occasionally observed, and they can last minutes before relaxation near room temperature (5). This result suggests that the energy difference between occupying T_4 and H_3 sites is much smaller for Pb than for Ge adatoms. Because of the weakness of the Pb–Ge bond relative to the covalent Ge–Ge bond and the much longer H_3 site lifetime of Pb atoms compared with Ge adatoms, structural changes of Ge adatoms in the lightly Pb-doped surface occur at lower temperatures than in the pure Ge(111) surface.

Adatom row shifts. On the lightly Pb-doped Ge(111)- $c(2 \times 8)$ surface, the Ge adatoms in the same row can shift in concert along the row by one primitive vector of the substrate and trap a Pb atom on a surface interstitial site (H_3). Some time later, the structure can relax (5). We present a detailed mechanism for the creation and annihilation of this metastable structural excitation on the basis of our new

STM observations.

An example of the $c(2 \times 8)$ structure with a substitutional Pb atom is shown schematically in Fig. 4A. The Pb atom hops rapidly between the T_4 site and neighboring metastable H_3 sites near room temperature. The Ge adatoms also hop in a similar way but at a much slower rate because of higher activation energies. While the Pb atom has hopped to the left H_3 site, there is a chance that Ge adatom 1 will hop left to a T_4 site through a metastable H_3 site (Fig. 4B). The Pb atom is then trapped on the H_3 site because there are no RADaBs available at any neighboring site. Adatom 2 may also move left through an H_3 site to a new T_4 site (Fig. 4C) because several RADaBs to its left are available for bond switching during the adatom motion. The process can proceed, and adatom 3, adatom 4, and so forth move left one by one in the same manner as adatoms 1 and 2. The result is a metastable structure like Fig. 4D, which has been observed previously (5). We call the above process a “vacancy-mediated” row shift because it features the propagation of a partial vacancy along the adatom row. It is analogous to vacancy diffusion in bulk material. The propagation normally ends at a domain boundary or a preexisting point defect.

The vacancy is “partial” because it is smaller than that which would be created by removing one adatom, as can be seen by inspection of Fig. 4. Likewise, the Pb adatom trapped on an H_3 site may be viewed as a “partially interstitial” atom. To limit cumbersome notation, we will refer to this simply as an “interstitial H_3 site” atom.

The metastable structure in Fig. 4D has been observed to relax back to that in Fig. 4A after a period of time. The relaxation is interpreted as another type of adatom row shift, which we call an “interstitial-site-mediated” row shift. For the structure in Fig. 4D, the interstitial H_3 site Pb atom can move back to its original substitutional T_4

site while Ge adatom 1 hops right to an H_3 site (Fig. 5A). Adatom 1 is then trapped on the H_3 site. It has a chance to move right to a T_4 site if adatom 2 hops right to an H_3 site (Fig. 5B). In a similar manner, the trapped adatom 2 can move right to a T_4 site if adatom 3 hops right to an H_3 site (Fig. 5C). The process can continue until the structure relaxes back to the original structure (Fig. 5D). This adatom row shift is characterized by the propagation of an interstitial H_3 site as new Ge adatoms are sequentially trapped. It is similar to a series of the interstitialcy or kick-out mechanisms in bulk material.

Direct observation of a partial vacancy or of an interstitial H_3 site Ge atom would be strong evidence for the mechanisms proposed above. However, the small size of the point defects, their low concentration, and their high mobility make such observations very difficult.

We observed the propagation of an interstitial H_3 site Ge atom along the row by carefully tuning the data acquisition conditions. Two consecutive 70 \AA by 75 \AA STM images, taken 51 seconds apart at $\sim 70^\circ\text{C}$ are shown in Fig. 6. In Fig. 6A, an adatom row shift is occurring in the row indicated by the arrow below the image. Some atoms appear as incomplete circles because of Ge adatom motion during data acquisition; that is, the atom is in one position when we start to scan it and moves to a new position before we finish. In the same row, below the “incomplete” atoms, is an interstitial H_3 -site Ge adatom like adatom 3 in Fig. 5C. In Fig. 6B, the interstitial H_3 site propagates along the row. An interstitial-site-mediated row shift is occurring. Each Ge adatom stays trapped on the interstitial H_3 site for only seconds or less before the structure propagates. The adatom structure on one side of the interstitial H_3 site Ge adatom is in 2×2 local order, and that on the other side is in $c(2 \times 4)$ local order, exactly as was observed previously around

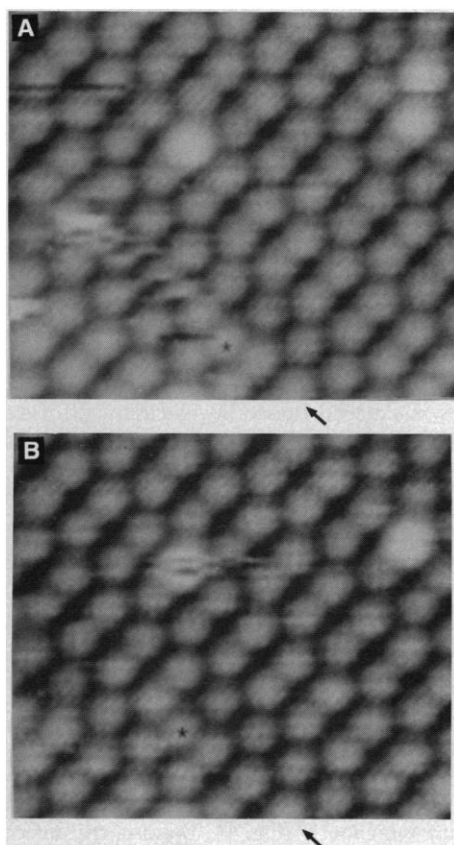
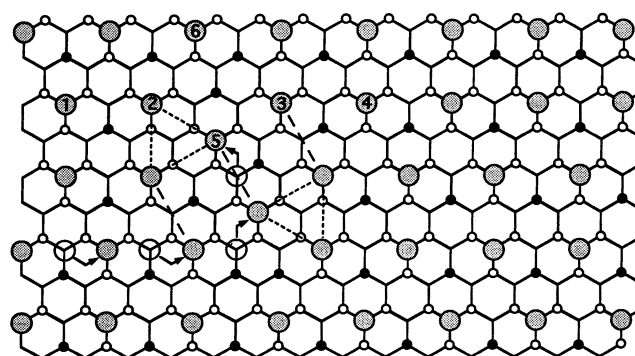


Fig. 6. Two consecutive 70 \AA by 75 \AA STM images of an interstitial-site-mediated row shift occurring in the row labeled with an arrow. Sample at $\sim 70^\circ\text{C}$, images taken at (A) $t = 0 \text{ s}$ and (B) $t = 51 \text{ s}$. Dark and bright atoms are Ge and Pb atoms, respectively. The Ge adatoms trapped on an H_3 site are marked with an asterisk.



● Ge adatom
○ Ge adatom before the motion

Fig. 7. Schematic representation of an excitation that broke the row structure locally. Atom numbers correspond to those in Fig. 4C. Coarsely dashed lines show the row direction of the new structure; finely dashed lines mark regions of local $\sqrt{3} \times \sqrt{3}$ order. The arrows indicate the motions required to convert to this structure from the one in Fig. 4C.

an interstitial H_3 site Pb adatom (5).

Although row shifts were seen in about 100 of our STM images, interstitial H_3 site Ge atoms were only directly observed in about 10 of the more than 1000 images analyzed. They were always accompanied by evidence of row shifts ("incomplete" atoms) in subsequent images. The characteristic local structure of a vacancy-mediated row shift (Fig. 4, B or C) was not observed, but this complementary process is required to explain atomic motions observed in this system. A partial vacancy probably migrates much faster than an interstitial H_3 site, so a vacancy-mediated row shift always appears in STM images as a chain of Ge adatoms moving along the row direction simultaneously. This result is not surprising because vacancies and interstitial atoms also have different diffusion coefficients in the bulk (2).

For clarity, the propagation of a partial vacancy and an interstitial H_3 site Ge adatom in Figs. 4 and 5 were drawn in one direction only. Actually, they can propagate back and forth along the adatom row, and STM images such as the "incomplete" Ge adatoms seen in Fig. 6A indicate this back and forth migration.

Nucleation of the metastable, rotated row structure. Although most atomic motions in

the $c(2 \times 8)$ reconstruction occur along the adatom rows, we also observed metastable excitations that break the row structure locally (Fig. 7). A small domain of the $2 \times$ row structure formed with its adatom rows running in a different $\langle 01\bar{1} \rangle$ direction from the original one. It formed within a single large region of $c(2 \times 8)$ and disappeared again in the following image. The arrangement can be explained as follows. Consider again the case of Fig. 4C. Adatom 5 (or adatom 6) can hop into the partial vacancy before adatom 3 moves, thus stopping the row motion. The hop also leaves behind a partial vacancy, which allows further motions of surrounding adatoms. The partial vacancy propagates downward and then moves away along another adatom row (indicated by the arrows in Fig. 7). Because the effect of the two types of defects is complementary, this structure could also be formed by an interstitial-type row shift entering on the lower row, turning upward, and then propagating away along the upper row. At the boundary between the new and the original domains of the row structure, there are local structures with two neigh-

boring RADaBs and with three Ge adatoms in the $\sqrt{3} \times \sqrt{3}$ configuration. These local structures are commonly observed at domain boundaries of $c(2 \times 8)$.

The formation of a rotated domain of the row structure inside a large, perfect domain of $c(2 \times 8)$ was observed only twice out of more than 1000 images. The surface relaxes back to the original row structure after a period of time. The rarity of this second kind of metastable excitation relative to the adatom row motions indicates that it is more energetically favorable for adatom 3 in Fig. 4C to move than it is for adatom 5, even though both make a similar $T_4 \rightarrow H_3 \rightarrow T_4$ motion. Essentially, a mobile point defect has a lower activation energy to propagate along the adatom row than away from it. Out-of-row motion becomes more probable at high temperature, however, and we believe that this is the mechanism by which new domains of the row structure can nucleate within preexisting domains, leading to the loss of long-range adatom order at high temperatures on the pure Ge(111) surface.

A small, rotated domain of the row structure is more likely to form near defects on the Ge(111) surface than inside a perfect domain of $c(2 \times 8)$. For example, there are immobile defects that appear to be dark in unoccupied-state tunneling images but bright in the occupied-state images. These defects are like those observed by Klitsner *et al.*, who found that areas on the Ge(111) surface that had reacted with oxygen appeared dark in unoccupied-state images but bright in occupied-state images (20). We conclude that the defects are caused by reactions with residual gas atoms from the vacuum chamber that passivate a few RADaBs. There are three reasons: (i) They are similar to the defects caused by oxidation; (ii) their density is found to increase with time; and (iii) they are immobile near room temperature (they can move at high temperatures but are still much less mobile than Ge adatoms). The Ge adatoms move around these defects rather than occupy them because RADaBs are no longer available there. Thus, the immobile defects can deflect the mobile point defects out of their original row, giving rise to the rotated row structure.

Three consecutive tunneling images of structural changes occurring around an immobile defect at 60°C are shown in Fig. 8. The atomic positions can be determined unambiguously (Fig. 9). Because the defect is not mobile, it can be used as a reference for the motions. Between Figs. 9A and 9B, the Pb atom marked with a "s" moves down from an H_3 site to another H_3 site (a long jump) and a Ge adatom moves up from a T_4 site to another T_4 site through the H_3 site in between. The Pb atom marked with an "x" also moves into the image through a

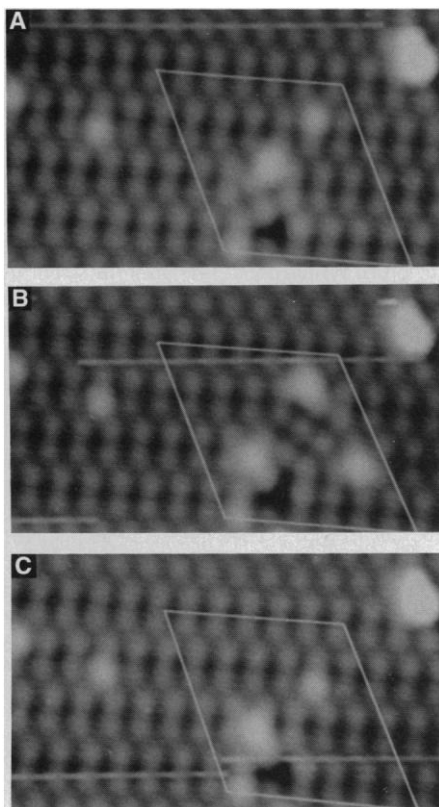


Fig. 8. Three consecutive 115 Å by 70 Å STM images of structural changes, taken at (A) $t = 0$ s, (B) 82 s, and (C) 167 s. The regions inside the solid lines are analyzed in Fig. 9.

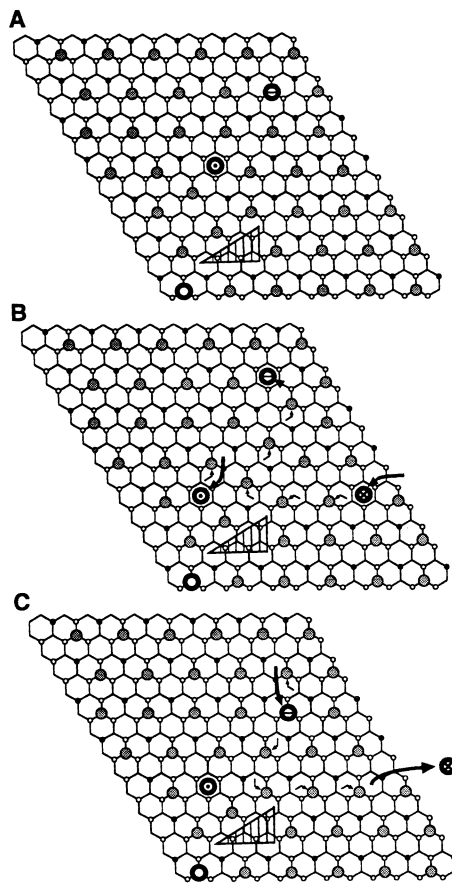


Fig. 9. Model for structural changes occurring in Fig. 8. The arrows are drawn assuming only that Ge adatoms hopped to nearest-neighbor sites with available RADaBs. As in Fig. 8, the models correspond to (A) $t = 0$ s, (B) 82 s, and (C) 167 s.

long jump and occupies an H_3 site. This motion is accompanied by a series of Ge adatom motions like those shown in Fig. 7. The motion of these Ge adatoms traps the Pb atom marked with a "—" on an H_3 site. Between Figs. 9B and 9C, Pb atom "x" leaves this region through another long jump and Pb atom "—" makes a long jump down to a T_4 site. A series of Ge atom movements occurs either because of the propagation of the partial vacancy created by the departure of Pb atom "x" or, alternatively, because of the propagation of an interstitial H_3 site from Pb atom "—."

Energetics on the Pure Ge(111) Surface

We can compare the energetics of various structures on Ge(111) by analyzing their frequency of occurrence in our tunneling images. In order of decreasing stability, these structures are $c(2 \times 8)$, other row structures, adatoms in $\sqrt{3} \times \sqrt{3}$ configurations or RADaBs on two neighboring first-layer atoms, and finally, interstitial H_3 site atoms and partial vacancies. The $c(2 \times 8)$ reconstruction is the ground state structure on Ge(111), and most of the area we see is in this configuration. However, as seen in Fig. 1, extra adatom rows are occasionally seen on the Ge(111) surface at room temperature and result in three rows in local 2×2 or $c(2 \times 4)$ order. Three rows of 2×2 must be more stable than three rows of $c(2 \times 4)$ because the former structure is much more abundant in our tunneling images than the latter. Large domains of the row structure are more stable than small ones. At the boundaries between differently rotated domains of the row structure, we see local structures with three Ge adatoms in a $\sqrt{3} \times \sqrt{3}$ configuration or with two neighboring RADaBs. These structures exist only at domain boundaries, and thus, it can be concluded that they are not very favorable compared to the row structures. Even at the domain boundaries, structures with more than three $\sqrt{3} \times \sqrt{3}$ adatoms are rarely seen.

Structures with more than two neighboring RADaBs are vacancy-like point defects and are very unstable. Such partial vacancies, along with interstitial H_3 site atoms, are responsible for structural changes on Ge(111). The rate at which they propagate can be estimated from our STM images. The configuration with an interstitial H_3 site Ge adatom must have a lifetime of seconds or only slightly less to be visible in STM images taken at 70°C (Fig. 6). Thus, we estimate that the activation energy for the propagation of an interstitial H_3 site along the row is around 0.8 eV. The lifetime of a partial vacancy must be even shorter because our scan speed is too slow to detect its propagation. The activation energy for the propaga-

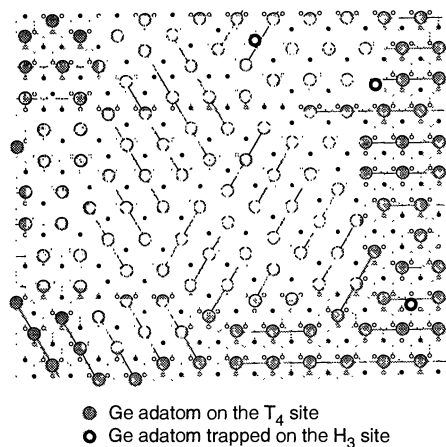


Fig. 10. Model of a snapshot of a possible configuration of the high-temperature 1×1 phase. The row direction of each domain is marked.

tion of a partial vacancy must therefore be less than 0.65 eV.

The creation of these two mobile point defects is thermally activated. Within a domain of the $2 \times$ row structure, partial vacancies and interstitial H_3 site atoms are formed in pairs. To create a partial vacancy-interstitial pair within a row, an atom must jump to an H_3 site and its neighbor must be available to trap it there, by the mechanism illustrated for a Pb atom in Fig. 4B. We can estimate the formation energy of the pair in a perfect region of Ge(111)- $c(2 \times 8)$. The mean lifetime for a Ge adatom to stay at the T_4 site is (from Eq. 1 and the discussion preceding it) $10^{-13} \exp(0.8/k_B T)$ s and its lifetime on the H_3 site is $10^{-13} \exp(0.2/k_B T)$ s. The generation rate for the partial vacancy-interstitial pair is given by the product of three terms: (i) the rate at which an atom jumps to an H_3 site, (ii) the probability that a neighboring atom is on an H_3 site and thus available to trap the first atom, and (iii) a geometrical factor of order 0.1 because there are at least two H_3 sites available for each jump. The rate at which an atom jumps to an H_3 site is the inverse of its lifetime on the T_4 site, $10^{13} \exp(-0.8/k_B T)$ s^{-1} . The probability that another atom will be on an H_3 site is the ratio of its lifetime on the H_3 site to that on the T_4 site, which is $\exp(-0.6/k_B T)$. Therefore, the interstitial-vacancy pair generation rate is about $10^{12} \exp(-1.4/k_B T)$ s^{-1} per atom. Thus, the formation energy for the pair in perfect $c(2 \times 8)$ is ~ 1.4 eV (21).

Because perfect $c(2 \times 8)$ is the ground state structure on Ge(111), the formation energy of mobile defects will be lower at domain boundaries and in other regions of the surface that are not in a perfect $c(2 \times 8)$ configuration. For example, we observe shifts much more frequently in adatom rows

next to an extra row (such as the one indicated by an arrow in Fig. 1) than in a perfect $c(2 \times 8)$ domain. Likewise, more atomic motions occur near domain boundaries. This assumption is reasonable, based on our discussion of the stability of various structures. Because the configuration at the domain boundaries is a less favorable one than the $2 \times$ row structures, the barrier for an adatom there to hop to an H_3 site is less than that for an adatom in perfect $c(2 \times 8)$. Thus, we expect the activation energy for creation of mobile point defects at domain boundaries will be less than 1.4 eV, and adatom motion will occur at boundaries at a lower temperature than it will inside large domains.

Phase Transition of Ge(111)- $c(2 \times 8) \leftrightarrow 1 \times 1$ at $\sim 300^\circ\text{C}$

The creation and propagation of partial vacancies and interstitial H_3 site atoms may lead to the $c(2 \times 8) \leftrightarrow (1 \times 1)$ phase transition on Ge(111). This transition has been studied by a number of techniques, but the detailed mechanism responsible for the formation of the high-temperature 1×1 phase is still not well understood. Phaneuf and Webb did a detailed study of the phase transition using LEED (22). They observed that above the transition temperature ($\sim 300^\circ\text{C}$), the eighth-order and fourth-order peaks disappeared and half-order peaks broadened, split, and decreased in intensity with increasing temperature. The average domain size decreased from about 37 to about 17 Å as the temperature increased from 300° to 600°C (22). A later He diffraction study confirmed many of these observations (23). A core-level study of the phase transition by Aarts *et al.* indicated that no significant changes occur in either the binding energies or in the relative intensities of the two surface components (17), which implies that the ordered adatom structure becomes disordered without an appreciable change in the number of adatoms present or in the nature of their binding to the first-layer atoms. Photoelectron diffraction, ellipsometry, and LEED studies also showed that the local adatom structure was unchanged during the phase transition (22, 24, 25). A recent direct STM observation by Feenstra *et al.* showed that the transition is caused by adatom diffusion (7). However, the atomic motions in the disordered 1×1 phase are very fast, and thus, the detailed structure in the 1×1 phase could not be resolved. The disordered region started from the domain boundaries of $c(2 \times 8)$ at $\sim 200^\circ\text{C}$ and grew continuously with the temperature until the entire surface became disordered at 300°C . They also observed that some of the adatom rows in the $c(2 \times 8)$ reconstruction become

"fuzzy." We also studied the clean Ge(111) surface up to $\sim 200^\circ\text{C}$. We observed rapid adatom motions at domain boundaries and fuzzy rows, consistent with their results (7). We also occasionally observed the nucleation of a region of rotated row structures.

All of these results can be explained in terms of the creation and propagation of mobile point defects on the Ge(111)- $c(2\times 8)$ surface and the row shifts and the nucleation of rotated domains of $c(2\times 8)$ to which they lead. As the temperature increases, more of the mobile point defects are created. In the last section, we calculated the formation energy for the interstitial site-vacancy pair in perfect $c(2\times 8)$ to be 1.4 eV. The generation rate is then estimated to be on the order of 10^{-13} , 10^{-7} , 10^{-3} , and 1 s^{-1} per atom at 25° , 100° , 200° , and 300°C , respectively. These estimates indicate that the effects of Ge adatom motions can be observed near 200°C and that at 300°C they would be too fast for the STM to image, which agrees well with experimental observations (7). Because of the much higher propagation rate of the partial vacancy compared with that of an interstitial H_3 site, it is likely to be the dominant cause for the structural changes occurring on this surface.

We therefore propose that the surface structure at high temperature ($>300^\circ\text{C}$) is composed of small domains (tens of angstroms in diameter) of the $2\times$ row structures, which have row directions in any one of the three possible $\langle 01\bar{1} \rangle$ directions. Inside the domains, there are adatom row shifts occurring as a result of the propagation of the two types of mobile point defects that are mainly created at domain boundaries, consistent with STM results (7). At a fixed temperature, one domain can grow at the expense of another, but the average size remains constant. As the temperature is increased, the excitation that forms a new domain of rotated row structure becomes more probable, and the average size of the domains shrinks, as observed in LEED (22). As the ordered $c(2\times 8)$ regions disappear at $\sim 300^\circ\text{C}$, the $8\times$ and $4\times$ periodicity is lost, but the $2\times$ periodicity of the row structure is still present, in agreement with LEED and He diffraction (22, 23).

The structure of a possible configuration in the high-temperature 1×1 phase (Fig. 10) is somewhat disordered and composed of domains of the row structure. Between domains there are local structures of $\sqrt{3}\times\sqrt{3}$ and of two neighboring RADaBs. There are also local structures with an adatom trapped on the interstitial H_3 site and with a high density of RADaBs, and they become more abundant

with increasing temperature. The 2×2 has threefold symmetry, and its row direction can be assigned to any one of the three possible $\langle 01\bar{1} \rangle$ directions. The incommensurate structure proposed by Phaneuf and Webb, which is composed of domains of 2×2 separated by walls in the $c(2\times 4)$ local arrangement (22), is a special case of this model. Therefore, the main features of the diffraction pattern can be expected to be similar for both models. However, our model additionally explains the growth of the disordered region from domain boundaries between 200° to 300°C , the change in average domain size with increasing temperature, and the "fuzzy" rows. Furthermore, it provides a mechanism, the motion of mobile point defects, for the transition from the $c(2\times 8)$ reconstruction to the high-temperature phase.

Feenstra *et al.* observed that the disordered region forms a band with a fixed average width between two translationally inequivalent domains of $c(2\times 8)$, which is in equilibrium with the ordered domains (7). We believe that the surface stress caused by large domains of the $c(2\times 8)$ reconstruction is responsible for the stabilization of the disordered region below 300°C and for the continuous growth of the disordered region from 200° to 300°C . Spectroscopic ellipsometry by Abraham *et al.* suggested that the surface stress plays a role in the phase transition (24). An important role for surface stress in this transition would be consistent with observations of phase transitions on other semiconductor surfaces, such as the Si(111)- 7×7 to 1×1 transition at $\sim 860^\circ\text{C}$ and the Pb/Ge(111) $\sqrt{3}\times\sqrt{3}$ to 1×1 transition at $\sim 180^\circ\text{C}$. In all three transitions, the disordered regions grow continuously with the temperature from a boundary: domain boundaries in the Ge(111) system, step edges on Si(111) (8, 26), and phase boundaries in Pb/Ge(111) (6). The bonding in semiconductors is strong and directional, and thus, a large domain of a surface reconstruction can generate significant stress in the underlying substrate. The stress can be expected to dramatically change the surface energetics at step edges, domain boundaries, or phase boundaries. Therefore, great care should be taken in the analysis of phase transitions on semiconductor surfaces when nonmicroscopic techniques are used.

Conclusion

We have presented a microscopic mechanism for adatom motions on Ge(111). The fundamental units responsible for these motions are the two complementary types of

mobile point defects: an interstitial H_3 site Ge adatom and a partial vacancy. The Ge(111)- $c(2\times 8)\leftrightarrow(1\times 1)$ phase transition is explained by the generation and propagation of these two types of mobile point defects. Thus, very complex and beautiful transformations can arise from the motions of two fundamental point defects.

REFERENCES AND NOTES

1. B. S. Bokshtein, S. Z. Bokshtein, A. A. Zhukhovitskii, *Thermodynamics and Kinetics of Diffusion in Solids* (American Publishing, New Delhi, India, 1985).
2. W. Frank, U. Gösele, H. Mehrer, A. Seeger, in *Diffusion in Crystalline Solids*, G. E. Murch and A. S. Nowick, Eds. (Academic Press, London, 1984), chap. 2.
3. M. G. Lagally, *Phys. Today* **46**, 24 (November 1993), and references therein.
4. E. Ganz, S. K. Theiss, I.-S. Hwang, J. Golovchenko, *Phys. Rev. Lett.* **68**, 1567 (1992).
5. I.-S. Hwang and J. Golovchenko, *Science* **258**, 1119 (1992).
6. ———, *Phys. Rev. Lett.* **71**, 255 (1993).
7. R. M. Feenstra *et al.*, *ibid.* **66**, 3257 (1991).
8. S. Kitamura *et al.*, *Nature* **351**, 215 (1991).
9. M. Harsen, *Constitution of Binary Alloys* (McGraw-Hill, New York, 1958), p. 771.
10. J. J. Metois and G. Le Lay, *Surf. Sci.* **113**, 422 (1983).
11. R. S. Becker, J. A. Golovchenko, B. S. Swartzentruber, *Phys. Rev. Lett.* **54**, 2678 (1985).
12. R. Feidenhansl *et al.*, *Phys. Rev. B* **38**, 9715 (1988).
13. R. S. Becker, B. S. Swartzentruber, J. S. Vickers, T. Klitsner, *ibid.* **39**, 1633 (1989).
14. T. Klitsner and J. S. Nelson, *Phys. Rev. Lett.* **67**, 3800 (1991).
15. N. Takeuchi *et al.*, *ibid.* **69**, 648 (1992).
16. R. M. Feenstra and A. J. Slavin, *Surf. Sci.* **251-252**, 401 (1991).
17. J. Aarts, A.-J. Hoeven, P. K. Larsen, *Phys. Rev. B* **38**, 3925 (1988).
18. N. Takeuchi *et al.*, *ibid.* **49**, 10757 (1994).
19. The energy of a Ge-Ge bond is 1.6 eV in the bulk (27). A jump involving the breaking of two Ge-Ge bonds would presumably have an activation energy greater than 1.6 eV. It would be less than 3.2 eV, however, because of lattice relaxation and charge transfer during the movement.
20. T. Klitsner, R. S. Becker, J. S. Vickers, *Phys. Rev. B* **44**, 1817 (1991).
21. This activation energy will be less on Pb-doped surfaces, because Pb jumps more readily to H_3 and has a longer lifetime there, so it can be readily trapped. Additionally, long jumps of Pb atoms can leave behind a vacancy in one row and create an interstitial defect in another.
22. R. J. Phaneuf and M. B. Webb, *Surf. Sci.* **164**, 167 (1985).
23. J. S. Ha and E. F. Greene, *J. Chem. Phys.* **91**, 7957 (1989).
24. M. Abraham, G. Le Lay, J. Hila, *Phys. Rev. B* **41**, 9828 (1990).
25. L. Pattthey, E. L. Bullock, K. Hricovini, *Surf. Sci.* **269-270**, 28 (1992).
26. N. Osakabe, Y. Tanishiro, K. Yagi, G. Honjo, *ibid.* **109**, 353 (1981).
27. C. Kittel, *Introduction to Solid State Physics* (Wiley, New York, ed. 5, 1976), p. 94.
28. We acknowledge helpful discussions and criticism of the manuscript by E. Kaxiras and S. D. Theiss. Supported by the Materials Research Laboratory at Harvard University (contract NSF-DMF-8920490) and the Joint Services Electronics Project (contract N00014-89-J-1023).